Comparison of static and dynamic pore compressibilities in carbonate rocks

Marco Ceia, Roseane Misságia, Irineu Lima Neto, Alexandre Bastos Jr., Lorena Figueiredo, Grazielle Oliveira, UENF/LENEP

This paper was prepared for presentation during the 14th International Congress of the Brazilian Geophysical Society held in Rio de Janeiro, Brazil, August 3-6, 2015.

Abstract

Pore volume compressibility is one of the main properties in reservoir simulations and can be obtained using logging and seismic data, which is a dynamic approach; however, for reservoir simulations, results derived from static measurements are more reliable, once small scale features as micro-cracks can make the dynamic results be underestimated. This study compares the evaluation of pore volume compressibility in carbonate rocks by two different techniques in hydrostatic conditions; one uses radial and axial deflections measured with a cantilever and LVDT's to estimate the volumetric changes of each effective pressure in static conditions. The other technique estimates pore compressibility from dynamic measurements, i.e., P- and S- wave velocities. Using both results, it was possible to obtain correlations between static and dynamic pore volume compressibilities for each sample.

Introduction

The mechanical properties of rocks are the key point for a variety of activities related to the hydrocarbon industry, such as drilling, completion, wellbore design and reservoir management for production optimization as to avoid unexpected interventions. Rock characterization during the formation productive life allows the evaluation of different production scenarios, bringing relevant information for improvement of reserves' estimation reliability. The energy that drives hydrocarbon production is a consequence of external pressure created by overburden pressure acting on the reservoir rock while the internal pressure is applied to the grains by the confined fluid. The equilibrium of these pressures is kept until the production is started, when internal pressure decreases and effective pressure increases, since the reservoir fluids become less effective in opposing the weight of the overburden and pores are compressed by additional formation compaction. Therefore, this behavior needs to be considered in reservoir characterization because they commonly affect rock porosity and if neglected can result in erroneous analysis of reservoir behavior, recoverable volume and driving mechanism (Tiab and Donaldson, 2004). Pore compressibility can also be used to calculate produced oil volume, gas and/or water during each production stage.

Several researchers conducted a series of theories and analysis attempting to obtain approximate values of pore compressibility. Geertsma (1957) did a remarkable work on the comprehension of the pressure-volume relationship in porous reservoir rocks, developing equations for a better understanding of bulk and pore volume. He introduced the concept of three types of compressibility: bulk (C_b), matrix (C_m) and pore (C_p). The determination of C_b and C_m uses relatively simple techniques of rock volumetric deformation.

The static experimental determination of C_p can be obtained through two different approaches. One is to evaluate pore compressibility as a porous pressure function, "simulating" the production process of a reservoir, in which as the depletion occurs, the pore volume is reduced. In those experiments the confining pressure is usually kept constant. This type of pore compressibility is usually referred as C_{pp}. The other approach is to measure the porous space variation when the sample is submitted to different confining pressures, but keeping pore pressure steady. This type is referred as C_{pc} and is usually associated with the volumetric variation of rock samples when they are brought to surface after coring. Despite the phenomenological differences between those two compressibilities, both are dependent on effective pressure and can be related one to another (Jaeger *et al*., 2007). Zimmerman *et al.* (1986) re-derived the relationships between different compressibilities and in terms of the confining and pore pressure. The pore compressibility as a function of the confining pressure is defined as:

$$C_p = -\frac{1}{V_p}\left(\frac{\partial V_p}{\partial P}\right)_{Pp} \qquad (1)$$

Pore compressibilities can also be inferred using elastic wave velocities obtained from seismic surveys or well-logging data (Suman and Mukerji, 2009). Berge (1998) and Mavko *et al*. (2009) summarize the theoretical aspects of this methodology. This type of pore compressibility is often referred as dynamic and differs from the static measurements (Jizba (1991), Macini and Mesini (1998)) especially at low pressures. This difference tends to decrease as pressure increases and low aspect ratio pores tend to close.

This work aims to analyze and compare static and dynamic measurements of pore volume compressibility in carbonate rocks subjected to different confining pressures.

Method

The Rock Physics and Deformation system of UENF/LENEP (Fig. 1) was used for such static and dynamic measurements. That system consists of a triaxial (Hoek-Franklyn) core holder that enables radial confining pressure through hydraulic pumping silicon oil around a jacketed core plug. Axial compression can also be applied by a piston that can move a platen towards the base of the core plug. The top of the core plug moves another platen, pulling it against another a fixed part of the rig. Such compressive movement enables the axial loading. Pressure transducers are used to measure the radial pressure while a load cell is used to measure the strength of the force in which the rock sample is submitted. The system is also equipped with 3 pairs of ultrasonic transducers, which enables the measurement of P- and S-waves in three axes (X, Y and Z).

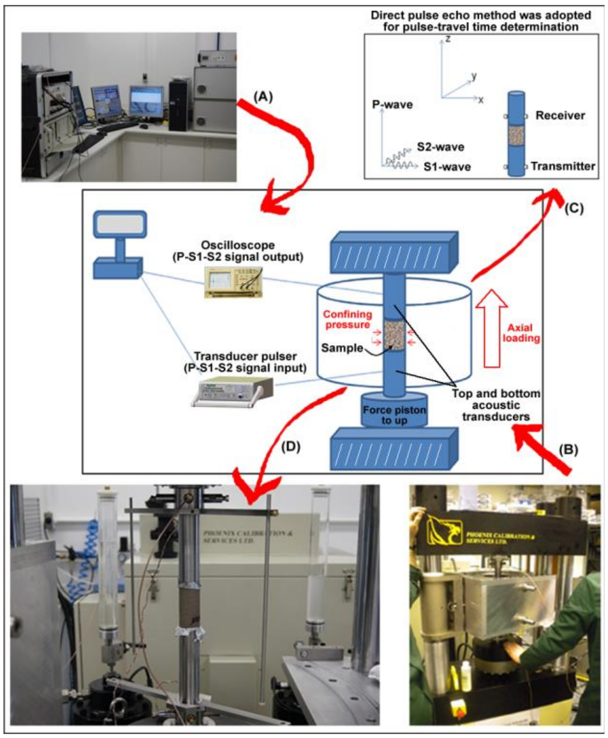

Figure 1-Diagram (central panel) and images of the Rock Physics and Deformation System.

LVDT's (Linear Variable Differential Transformer) allows the measurement of the axial deflection and a cantilever transducer provides the radial deflection. Those deflections are measured at 20 Hz sampling rate and are used to calculate axial and radial strain for each pressure stage.

Static Measurements

Equation 2 shows the relationship between the dry bulk modulus (K_{dry}), matrix (solid) bulk modulus (K_{ma}), porosity (ϕ) and dry pore stiffness (K_{phi}):

$$\frac{1}{K_{dry}} = \frac{1}{K_{ma}} + \frac{\phi}{K_{phi}} \tag{2}$$

The static evaluation of pore compressibility can be performed using Eq. 3 and substituting it back in Eq. 2, as shown in Eq. 4.

$$C_{pc} = \frac{1}{K_{phi}} \tag{3}$$

$$C_{pc} = \frac{\frac{1}{K_{dry}} - \frac{1}{K_{ma}}}{\phi} \tag{4}$$

The dry bulk modulus can be estimated using Eq. 5

$$K_{dry} = \frac{\Delta P}{\Delta V / V_o} \tag{5}$$

Where ΔP is the hydrostatic pressure variation, V_o is the original volume of the core sample that can be measured using a caliper, ΔV is the variation in the volume, which can be evaluated using the axial and radial deflections.

Matrix (solid) bulk moduli were estimated using Hill's average on Voigt and Reuss bounds of each mineral fraction (Mavko et al., 2009). Table 1 shows the values of mineral bulk modulus for each individual phase.

Table 1: Physical properties of the mineral phases according to Mavko et al. (2009).

Mineral Properties			
	K_{min} (GPa)	G_{min} (GPa)	ρ_{min} (g/cm³)
Calcite	70.76	30.34	2.71
Quartz	37	44	2.65
Dolomite	80.23	48.77	2.87
Sylvite	17.4	9.4	1.99
Fluorite	86.4	41.8	3.18

Dynamic Measurements

This approach uses P- and S-wave velocity measurements (v_p and v_S respectively) in different effective pressures to estimate dry bulk modulus (K_d) using equation 6. Later, pore compressibility can be estimated using Eq. 4.

$$K_{dry} = \rho_b \left[v_P^2 - \frac{4}{3} v_S^2 \right] \tag{6}$$

The experiments were performed in a nearly hydrostatic condition maintaining the axial stress approximately 1MPa higher than the confining pressure and the average was assumed as the effective pressure.

The Dataset

In this work, 6 carbonate samples extracted from USA outcrops were used. Three were extracted from Edwards Formation (labeled as Edwards Yellow, Edwards White and Desert Pink). Other samples used were Silurian Dolomite, Wisconsin Dolomite and Austin Chalk. Table 2 lists the mineral composition obtained from X-Ray Diffraction and Rietveld method (Rietveld, 1969) while Table 3 shows the results of Helium Porosimetry at ambient conditions.

Table 2- Mineral content of the rock samples evaluated from XRD measurements with Rietvield approach.

Sample	Edwards Yellow (EY)	Edwards White (EW)	Desert Pink (DP)	Austin Chalk (AC)	Wisconsin (W)	Silurian Dolomite (SD)
Calcite (wt %)	99.79	99.86	99.61	99.65	0.66	-
Quartz (wt %)	-	0.11	0.18	-	16.17	-
Dolomite (wt %)	-	-	0.12	-	81.93	100
Sylvite (wt %)	-	0.04	0.09	0.35	-	-
Fluorite (wt %)	0.21	-	-	-	-	-

Table 3: Petrophysical properties of the rock samples.

Sample	Grain Density (g/cm³)	Porosity (%)	Bulk Density (g/cm³)	Rock Type
AC-001	2.707	26.112	2.000	Austin Chalk
DP-001	2.692	25.474	2.006	Desert Pink Limestone
EW-002	2.689	11.046	2.392	Edwards White Limestone
EY-002	2.697	22.563	2.089	Edwards Yellow Limestone
SD-002	2.814	16.200	2.358	Silurian Dolomite
W-001	2.830	4.080	2.715	Wisconsin Dolomite

Results

An example of axial and radial deflection measurements is shown in Figure 2, for sample EY-002. All of the rocks exhibited a similar behavior, the axial deflection tending to increase with pressure whereas the radial deflection remains practically constant. The deflections were used to estimate the volumetric changes according to pressure, and then evaluate the dry bulk modulus.

Table 4 shows the results of the evaluation of the mineral moduli after using the Hill average. Using bulk and mineral moduli, it was possible to evaluate the pore compressibility according to Eq. 4 as shown in Figure 3 (static approach).

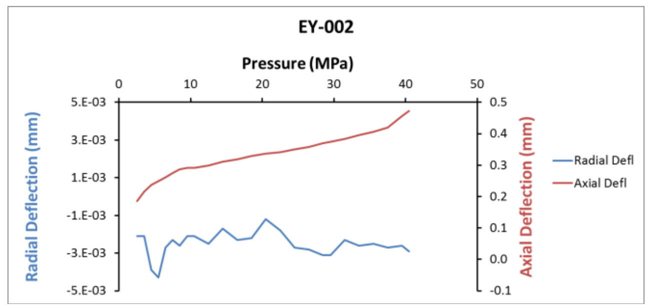

Figure 2: Graphic of the axial and radial deflections for sample EY-002.

Table 4: Mineral moduli evaluated using Hill average.

Sample	Kma (GPa)	Gma (GPa)
AC-001	70.29	30.19
DP-001	70.56	30.34
EW-002	70.65	30.33
EY-002	70.79	30.36
SD-002	80.23	48.77
W-001	70.16	47.80

Figure 4 shows the results of P-wave velocities for each pressure. The dolomites samples exhibited the higher velocity values. It is also possible to observe that the pressure increment affect the velocity in different ways in each of the rock samples. While for Austin Chalk and the limestones, the pressure increasing makes the velocity vary in a smooth way between 0 to 10 MPa, the dolomites showed a steeper variation within the same pressure range. For higher pressures, all of the samples exhibited a near-constant tendency.

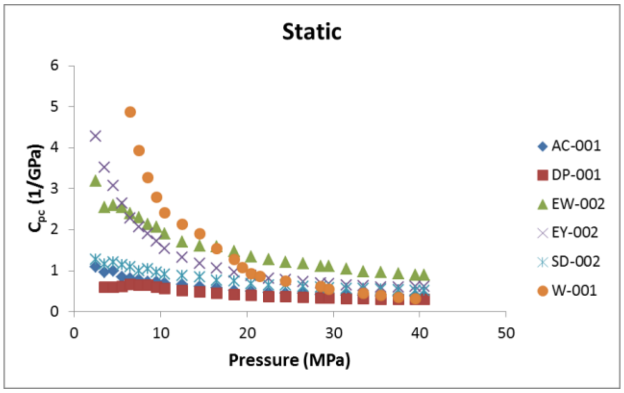

Figure 3: Pore compressibility results obtained using static measurements.

The shear wave velocity variation according to pressure is shown in Figure 5. The same behavior regarding the pressure increment that was observed in P-wave velocities can be noted for the S-wave velocities.

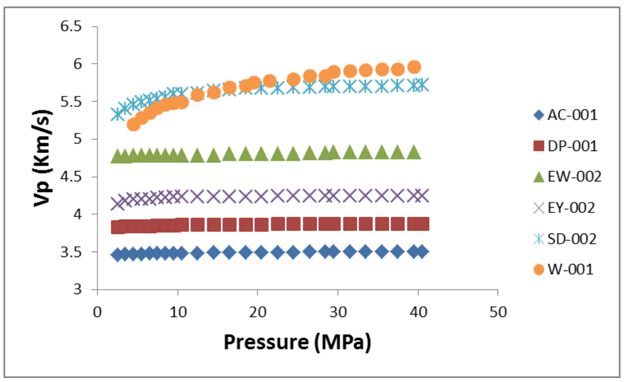

Figure 4: Crossplot of the P-wave velocity variation for each pressure step.

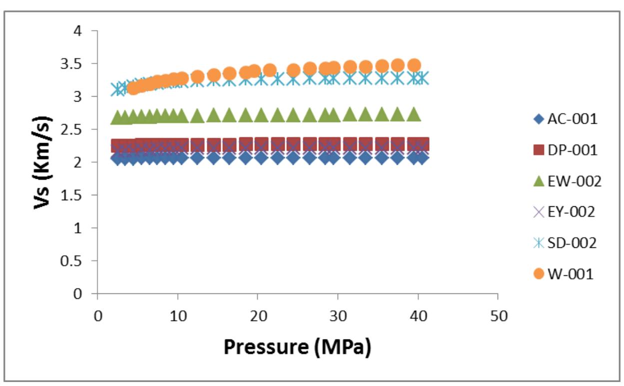

Figure 5: Crossplot of the S-wave velocity variation for each pressure step.

Those velocities were used to estimate the dry bulk modulus with a dynamic approach. Later, it was possible to use Eq. 4 to estimate the pore compressibility of the selected samples. Figure 6 displays such dynamic result.

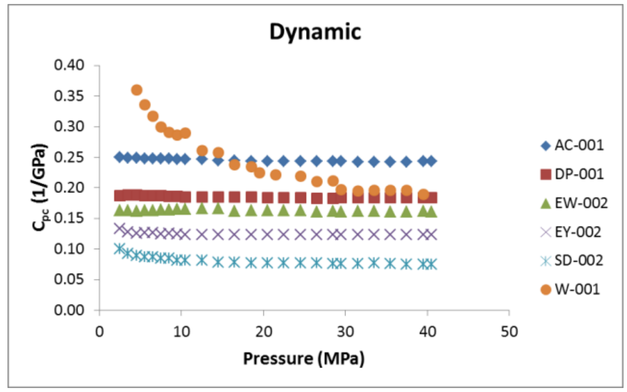

Figure 6: Pore compressibility results obtained using dynamic measurements.

A comparison between the static and dynamic results of the pore compressibility can be made plotting the ratio of dynamic value to the static value (Figure 7). If this ratio is 1, both estimates would be the same while lower ratio indicates higher discrepancies. For all of the samples, the increasing of the pressure is likely to increase that ratio. However, while AC-001, DP-001 and W-001 showed a steep increment, the other samples showed a smooth increasing.

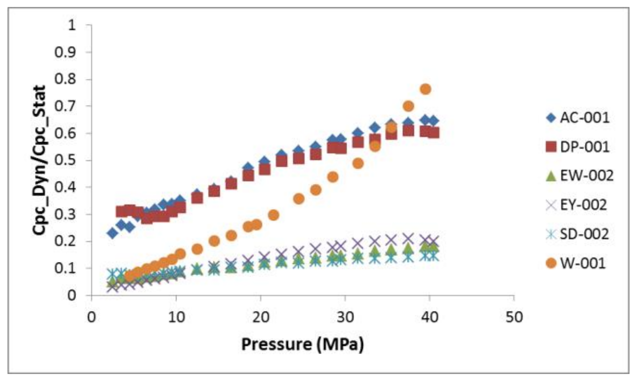

Figure 7: Ratio of dynamic and static estimates of pore compressibility.

Figure 8 shows second-order polynomial best fittings on the selected pressure range. For all of the samples, R^2 was higher than 0.9.

Discussion

The behavior of pore compressibility is different depending whether if it is evaluated in static approach or in dynamic approach. While in the first mode, the variation in pore compressibility as pressure increases are likely to be more dramatic, especially for pressures lower than 10 MPa, in the dynamic mode the variation is smoother, except for sample W-001. The pressure increment also makes the rocks less compressible.

Lafarge et al. (1997) studied the dynamic compressibility of air in porous structures and observed that the variation of compressibility as frequency increases may vary for different samples. King (1969) and Cheng and Johnston (1981) found that at low pressure, static bulk modulus are lower than the dynamic one. Walsh and Brace (1966)

concluded that the presence of highly compliant cracks affects static modulus differently than the dynamic. According to Jizba (1991) when the concentration of cracks is low, the static modulus approaches the dynamic value. In static measurements, the rock is stressed at a slower rate than in dynamic. Walsh (1965) pointed out that the frictional sliding along internal cracks as a possible mechanism and the small-amplitude cycling deformation induced by elastic waves is insufficient to trigger such sliding (Fjær, 2009). This way, dynamic modulus is not affected.
Figueiredo et al. (2014) used Mercury Intrusion Porosimetry to estimate pore throat radius distributions in samples similar to EY, DP and W. They reported that influence of pore throats with radius smaller than 1μm in the pore volume is higher for W than for EY, while DP exhibited an intermediate influence. Although no geometrical property like aspect ratio was described in this work, micro-cracks are commonly associated with such small size porosity and could explain the differences in the behavior of pore compressibilities for those rocks.

Conclusions

This work presented the results of pore compressibility measurements obtained using static and dynamic approaches in the same rock samples submitted to the same conditions of external pressure. Those results showed the differences between those two approaches for pressure increment. In all cases, the ratio between those two results tends to increase as pressure increases according to a second-order polynomial.

Frictional sliding along internal micro-cracks are supposed to be the main mechanism to cause the different behavior between the two approached for the studied rocks. The presence of micro-cracks in some of those samples can be associated to micro-porosity, which was reported in a previous work.

Acknowledgments

The authors would like to thank UENF/LENEP for the facilities provided to perform this work, ANP-PRH-20 and Petrobras-PRH-226 for financial support and scholarships. RM acknowledges FAPERJ for Jovem Cientista research grant. We are also grateful to Remilson Rosa, Luiz Abreu, Nathaly Archilha, Lucas Oliveira, Luan Castro and Flavio Souza for their collaboration during the experiments and analysis.

References

Berge, P.A. 1998. Pore Compressibility in Rocks. Biot Conference on Poromechanics. Louvain-la-Neuve, Belgium.

Cheng, C.H. and Johnston, D.H. 1981. Dynamic and static moduli. Geophys. Res. Lett., 8, 39-42. doi: 10.1029/GL008i001p00039

Figueiredo, L.A.B.; Misságia, R.; Ceia, M.; Archilha, N.; Lima Neto, I. Evaluation of pore system from outcrop rocks by Mercury intrusion porosimetry. Proceedings of the VII Symposium of the Brazilian Geophysical Society (SimBGf). Porto Alegre. Brazil.

Fjær, E. 2009. Static and dynamic moduli of a weak sandstone. Geophysics, 74**,**WA103-WA112. doi: 10.1190/1.3052113.

Geertsma, J. 1957. The effect of fluid pressure decline on volumetric changes of porous rocks. Petroleum Transactions, AIME, v. 210, p. 331–340.

Jaeger, J.; Cook, N.; Zimmerman, R. 2007. Fundamentals of Rock Mechanics. Wiley-Blackwell.

Jizba, D. 1991. Mechanical and Acoustical Properties of Sandstones and Shales. PhD. Thesis. Stanford University.

King, M.S. 1969. Static and dynamic elastic moduli of rocks under pressure. 11th U.S. Symposium on Rock Mechanics. American Rock Mechanics Association. Berkeley. California.

Lafarge, D., Lermanier, P., Allard, J.F. and Tarnow, V. 1997. Dynamic compressibility of air in porous structures at audible frequencies. J. Acoust. Soc. Am., 102, 4, October. doi:10.1121/1.419690

Macini, P. and Mesini, E. 1998. Static and Dynamic Reservoir Rock Compressibility at high pressure. 8th International Petroleum Conference and Exhibition. Society of Petroleum Engineers, SPE49549. Abu Dhabi, UAE.

Mavko, G., Mukerji, T. and Dvorkin, J. 2009. The Rock Physics Handbook. Cambridge: Cambridge University Press. 2nd edition.

Rietveld, K.M. 1969. A profile refinement method for nuclear and magnetic structures. J. Appl. Crystallogr., 2, p. 65-71.

Suman, A. and Mukerji, T. 2009. Uncertainties in rock pore compressibilities and effects on time lapse seismic modelling – An implication to Norne Field. 79th Annual International Meeting, SEG, Expanded Abstracts, 3909-3913. doi: 10.1190/1.3255684

Tiab, D. and Donaldson, E. 2004. Petrophysics. Theory and Practice of Measuring Reservoir Rock and Fluid Transport Properties. 2nd. Ed. Elsevier.

Walsh, J. 1965. The effect of cracks on the compressibility of porous rocks. J. Geophys. Res., American Geophysical Union, v. 70, n. 2, p. 381–389. doi: 10.1029/JZ070i002p00381

Walsh, J. and Brace, W. 1966. Elasticity of rock: a review of some recent theoretical studies. Rock Mechanics and Engineering Geology, 4. 283-297. International Society of Rock Mechanics. Springer-Verlag.

Zimmerman, R. W., Somerton, W. H., and King, M.S. 1986. Compressibility of porous rocks. J. Geophys. Res., 91, 12765–12777. doi: 10.1029/JB091iB12p12765

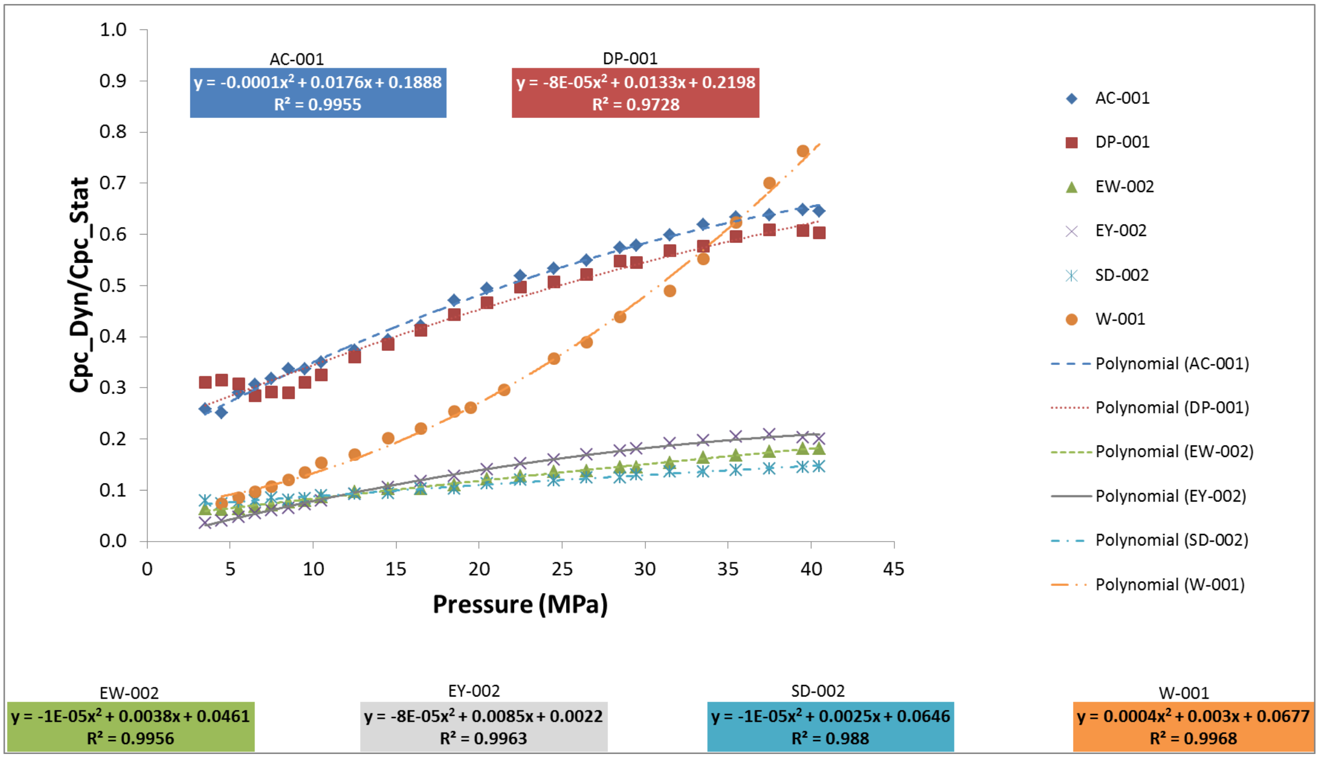

Figure 8: Second-order polynomial fittings of static to dynamic ratio of the pore compressibilities in a pressure range from 3.5 to 40.5 MPa.